Reprint: Morphological characterization of pulmonary microvascular disease in bronchopulmonary dysplasia caused by hyperoxia in newborn mice

原　著

東女医大誌 89(Extra1): E123-E133, 2019.7

Medical Molecular
https://doi.org/10.1007/s00795-018-0182-2

ORIGINAL PAPER

Morphological characterization of pulmonary microvascular disease in bronchopulmonary dysplasia caused by hyperoxia in newborn mice

Hidehiko Nakanishi[1] · *Shunichi Morikawa*[2] · *Shuji Kitahara*[2,3] · *Asuka Yoshii*[2,4] · *Atsushi Uchiyama*[1] · *Satoshi Kusuda*[1] · *Taichi Ezaki*[2]

Received: 15 November 2017 / Accepted: 21 January 2018

Abstract

Purpose Pulmonary microvascular injury is associated with the pathogenesis of bronchopulmonary dysplasia (BPD). To characterize the mechanisms of pulmonary vascular disease resulting from BPD, we studied the ultrastructural changes affecting pulmonary microvasculature.

Methods Newborn ICR mice were exposed to 85% hyperoxia or normoxia for 14 days, and then normal air replacement conditions for the following 7 days. At postnatal day (P)14 and P21, lungs were harvested for ultrastructural examination and assessment of pulmonary hypertension.

Results The ultrastructure of pulmonary microvasculature in the hyperoxia-exposed lungs revealed a collapsed capillary lumen. This was due to the abnormal morphology of endothelial cells (ECs) characterized by heterogeneously thick cytoplasm. Compared to normal air controls, the specimens displayed also remarkably thick blood–air barriers (BABs), most of which were occupied by EC layer components. Structural changes were accompanied by increased pulmonary artery medial thickness and right ventricular hypertrophy (RVH). Moreover, abnormalities in ECs persisted even after exposure to 7 days of normal air replacement conditions. Results were confirmed by morphometric quantification.

Conclusion Our results suggest that the abnormal morphology of capillary ECs and thick BABs correlates with pulmonary artery remodeling and RVH. These ultrastructural changes might represent possible mechanisms of secondary pulmonary hypertension in BPD.

Keywords Bronchopulmonary dysplasia · Hyperoxia · Newborn · Pulmonary hypertension · Pulmonary microvascular disease

Introduction

Bronchopulmonary dysplasia (BPD) is a chronic lung disease of prematurely born infants caused by oxygen toxicity, mechanical ventilation, and infection, and is characterized by decreased alveolarization and dysregulated development of the pulmonary microvasculature [1–3]. Above all, abnormal pulmonary microvascular injury might be linked to the pathogenesis of BPD [3], and in some cases of severe BPD, as shown in rodent models [4–7], impairments of developing pulmonary vasculature may cause serious pulmonary vascular diseases such as secondary pulmonary hypertension (PH), which contributes significantly to morbidity and mortality among prematurely born infants [8–11].

Microvascular injuries observed in BPD are generally demonstrated by abnormal immunohistochemical staining pattern and/or intensity of endothelial cell (EC) markers [4,

Electronic supplementary material The online version of this article (https://doi.org/10.1007/s00795-018-0182-2) contains supplementary material, which is available to authorized users.

✉ Hidehiko Nakanishi
hidehiko@qf6.so-net.ne.jp

[1] Department of Neonatology, Maternal and Perinatal Center Neonatal Division, Tokyo Women's Medical University, 8-1 Kawada-cho, Shinjuku-ku, Tokyo 162-8666, Japan

[2] Department of Anatomy and Developmental Biology, Tokyo Women's Medical University School of Medicine, Tokyo, Japan

[3] Department of Radiation Oncology, Harvard Medical School, Massachusetts General Hospital, Boston, MA, USA

[4] Department of Pharmacology and Experimental Therapeutics, Boston University School of Medicine, Boston, MA, USA

Published online: 23 January 2018

5, 12, 13], the barium angiogram technique, or scanning electron microscopy of corrosion casts [6, 14]. However, the actual morphological changes to the pulmonary microvasculature at the cellular level, including ECs, blood–air barriers (BABs), and other cellular components, in the injured developing lung remain poorly understood. A few early studies used electron microscopy to investigate pulmonary changes caused by hyperoxia [15–17] or administration of antiangiogenic compounds [18]; however, as these studies mostly investigated adult animal models or a different stage of BPD, limited information is available on the changes in the severely injured developing lung.

In this study, we sought to characterize the morphological changes in pulmonary vascular disease secondary to BPD caused by oxygen toxicity. To this end, we studied ultrastructural changes in pulmonary microvasculature, such as ECs and BABs, and assessed PH in response to injury to the developing lung in both the saccular and alveolar stages [19], using lungs from newborn mice exposed to hyperoxia for 14 days after birth followed by 7 days of normal room-air replacement conditions.

Materials and methods

Experimental design

Time-dated pregnant ICR mice were purchased from Japan SLC Inc. (Shizuoka, Japan). Within 12 h of birth, the pups from pairs of mothers were pooled and randomly divided into two litters that were continuously exposed to either air or 85% oxygen for 14 days (Air-14d and O_2-14d, respectively), and then to normal air replacement conditions for the following 7 days (Air-21d and O_2-Air 21d, respectively). During hyperoxic exposure, the mothers from paired litters were swapped every 48 h between air and oxygen conditions to diminish the effects of breathing high levels of oxygen. To expose the pups to hyperoxic conditions, a plastic case (34 cm × 24 cm × 24 cm) was prepared as an oxygen chamber, and oxygen was supplied with a home oxygen condenser (TO-90-7H; Teijin Pharma Ltd., Tokyo, Japan), which had an oxygen enrichment film for generating oxygen-rich gas from air. The oxygen concentration in the chamber was measured using an electrochemical analyzer (OX-21; Atom Medical, Tokyo, Japan). According to preliminary tests, the oxygen flow required to maintain an 85% oxygen concentration in the chamber was 4 L/min. The relative humidity and temperature in the exposure chamber were approximately 60% and 22 °C, respectively. The room was lighted for 12 h per day. The mice had continuous access to food and water, and their cages were cleaned every 4 days. All animal experiments were approved by the Animal Experiment Committee, Tokyo Women's Medical University (TWMU) (Approval number: AE17-40). Experiments were performed in accordance with the legislation of the Institute of Laboratory Animals for Animal Experimentation at TWMU.1.

Tissue preparation

To obtain lung samples, pups were weighed and then anesthetized with an intraperitoneal injection of a mixture of ketamine (87 mg/kg body weight) and xylazine (13 mg/kg body weight). After a thoracotomy to allow the lungs to collapse, the trachea was cannulated with a 0.61-mm outer-diameter polyethylene tube, the lungs were inflated with 4% paraformaldehyde in PBS at 22 cm H_2O pressure for 30 min, and the airway was ligated while the lungs were distended. The pup was then submerged in fixative for 1 day at 4 °C. Next, the lungs were dissected from the body and stored at 4 °C in PBS for subsequent processing and analyses. For cryosectioning, tissues were immersed in a graded series of sucrose in PBS (up to 30%) at 4 °C overnight. Subsequently, the tissues were embedded in Tissue-Tek O.C.T. compound (Sakura Finetek, Tokyo, Japan), snap-frozen in liquid nitrogen, and stored at − 80 °C. Cryosections (20 μm) were made on silane-coated glass slides, air-dried for at least 2 h, and immunostained. For paraffin sections, the tissues were embedded in paraffin after sequential dehydration in a graded ethanol series, and 6-μm-thick sections were prepared.

Transmission electron microscopy (TEM)

Lungs were rapidly dissected from anesthetized animals, cut into small pieces (~ 1 mm^3) in fixative solution composed of 2.5% glutaraldehyde in 0.1 M phosphate buffer (PB; pH 7.4), and further fixed in the same fixative at 4 °C for 24 h. After treatment with 1% osmium tetroxide in 0.1 M PB, the lung pieces were dehydrated in a graded series of ethanol aqueous solution and embedded in epoxy resin (epon 812 resin; TAAB Laboratories, Aldermaston, UK) using propylene oxide as the intermediate solvent. Epoxy 0.5-μm, semithin sections were stained with toluidine blue and examined under a light microscope for a quick check of lung structure after each treatment. The pieces were further sectioned into 70-nm-thick, ultrathin sections, contrasted with uranyl acetate and lead citrate, and examined under a Hitachi H-7000 electron microscope (Hitachi, Tokyo, Japan).

Analysis of lung structure

The degree of lung injury and its recovery during alveolar development was quantified using stereological methods and by determining the mean chord length (Lm), % air space volume density (% AVD), and secondary septal density, as reported previously [13]. To this end, we followed

a systematic sampling approach described by Tschanzand and Burri [20], and obtained three 0.044-mm^2 images from randomly oriented transverse sections of the left lung that excluded large airway and vascular structures. Lm was determined as described below using a BZ-9000 all-in-one microscope (Keyence Co., Osaka, Japan). First, six horizontal lines, 30 μm apart, were drawn in the section images, the length of the lines over airspaces between the intersections with alveolar walls was measured, the median length of one lung field was determined, and finally, the mean value was calculated using three fields per animal. Employing ImageJ [21] and a custom-written macro, % AVD was determined using the point counting method detailed by Weibel [22] on the basis of three fields per animal. Secondary septal density was determined using the Cell Counter tool in ImageJ on three fields per animal. Pulmonary image data were acquired and processed by an observer blinded to treatment and exposure group of the lung specimens. Hematoxylin and eosin (H&E)-stained sections of distention-fixed, paraffin-embedded left lung tissue were used for structural studies.

Immunofluorescence staining of endothelial cells

Cryosections were incubated in 5% Block Ace (Dainippon Seiyaku, Osaka, Japan) to avoid nonspecific staining and were successively incubated at 4 °C overnight with an anti-CD31 rabbit polyclonal antibody (1:100, ab15537; Abcam, Cambridge, UK) in PBS containing 1% BSA (Sigma, St Louis, MO, USA). After several washes with PBS, specimens were incubated with combinations of a fluorescent Cy3-conjugated anti-rabbit secondary antibody (1:200; Jackson ImmunoResearch, West Grove, PA, USA) for 1 h at room temperature. Immunostained sections were examined using a Leica TCS-SL confocal laser-scanning microscope (Leica Microsystems, Wetzlar, Germany). Negative controls, in which PBS was substituted for primary antibodies, were included for each tissue section.

Assessments of pulmonary microvasculature

% Fluorescent volume density (% FVD)

To quantify CD31 immunohistochemical results, the areal density of pulmonary microvascular cells in mouse pup lungs was analyzed using standard methods [22]. Using the systematic sampling method detailed above, immunofluorescence images of the peripheral lung were obtained, while avoiding the large airway and vessels. Following filtration and segmentation procedures, % FVD was determined by dividing the number of fluorescent pixels by the total number of pixels in the image [13]. Median % FVD of three images per pup lung section was used for analysis.

Ultrastructural measurement by TEM

Non-overlapping ultrathin section images were captured using Adobe Photoshop ver. 13.0.1. (Adobe Systems Inc. San Jose, CA, USA), and six capillaries in the alveolar wall per animal for each treatment group were analyzed. To quantify the ultrastructural features of pulmonary microvasculature, we measured and calculated the following four parameters.

- *BAB thickness (μm)* Total BAB thickness was measured on five different BAB portions per capillary, using the scale tool in Adobe Photoshop (version 13.0.1.). The mean of total BAB thickness from each group was used in the analysis.
- *Proportion of EC layer components in BAB (%)* The thickness of EC and alveolar epithelial cell (AEC) layer components in the BAB was measured, and the thickness of EC layer components relative to total BAB (%) was calculated. The mean value from each group was used in the analysis.
- *Thickness of EC cytoplasm (μm)* To quantify abnormal morphological changes EC cytoplasm in pulmonary capillaries, the thickness of five circumferentially different cytoplasmic portions per capillary was measured, and the mean from each group was used in the analysis.
- *Standard deviation (SD) of the thickness of EC cytoplasm* To quantify abnormal morphological changes in the EC cytoplasm in pulmonary capillaries, the SD of the thickness of five circumferentially different cytoplasmic portions per capillary was calculated, and the mean from each group was used in the analysis. High SD variance indirectly suggests that ECs have heterogeneously thick cytoplasmic components and a collapsed capillary lumen. Conversely, low SD variance suggests that ECs present a similar thickness circumferentially and that the capillary lumen is well preserved.

Assessments of pulmonary hypertension

Right ventricle (RV) hypertrophy

Hearts were removed and dissected to isolate the free wall of the RV from the left ventricle (LV) and septum (S). RV hypertrophy was calculated as the ratio of RV weight over LV + S weight (RV/[LV + S]) [23].

Arterial wall thickness

Vessel wall thickness was measured on pulmonary arteries (20–100 μm) associated with terminal and respiratory bronchioles on H&E-stained lung sections by an observer

blinded to the identity of the slides. Three vessels per pup lung were assessed for MT and external arterial diam- eter (ED). MT was expressed as the percentage of ED, MT% = [MT × 2 × 100]/ED.

Statistical analysis

Statistical analysis was performed using JMP® 12 software (SAS Institute Inc., Cary, NC, USA). Data are presented as means ± SDs, and treatment groups were compared using a factorial model of analysis of variance. When significant differences were detected, Dunnett's test for normal distribution or Steel–Dwass test for non-normal distribution was used as post hoc test with Air-14d or -21d as a control. Significance was determined at $P < 0.05$.

Results

Hyperoxic exposure is associated with disruption of alveolar development in the injured newborn lung

To evaluate morphological changes in alveolarization, we compared lung structures of animals exposed to hyperoxia for 14 days with those from animals subjected to hyperoxia followed by normal air replacement conditions for 7 days. Consistent with previous reports [4, 5, 7, 24–26], the peripheral airways of injured pup lungs exhibited a less complex interstitial structure and fewer secondary septa or alveoli than the lungs of air-breathing control pups. Even after exposure to normal air replacement conditions, the abnormal alveolar structures did not recover to control levels (Fig. 1). As shown in Supplementary Fig a–c, these structural changes were quantitatively confirmed by the Lm, % AVD, and secondary septal density.

Disruption of pulmonary microvasculature persists during the recovery phase

Exposure of newborn rodent lungs to hyperoxia causes abnormal pulmonary microvascular development [13, 24]. However, a little is known about the morphological changes to the pulmonary microvasculature, including ECs, BAB, and other cellular components. Here, we assessed the ultrastructural changes in the pulmonary microvasculature, as well as changes in staining pattern of the EC marker CD31 in each group (Air-14d, Air-21d, O_2-14d, and O_2-Air 21d). As shown in Fig. 2, microvascular EC staining was less abundant in hyperoxia-exposed (O_2-14d) than in air-exposed (Air-14d) lungs. Stereological quantification revealed that chronic exposure to 85% oxygen caused a decrease in % FVD of CD31-stained ECs in the periphery of injured lungs. In the lungs of pups allowed to recover under normal air replacement conditions (O_2-Air 21d), % FVD remained low

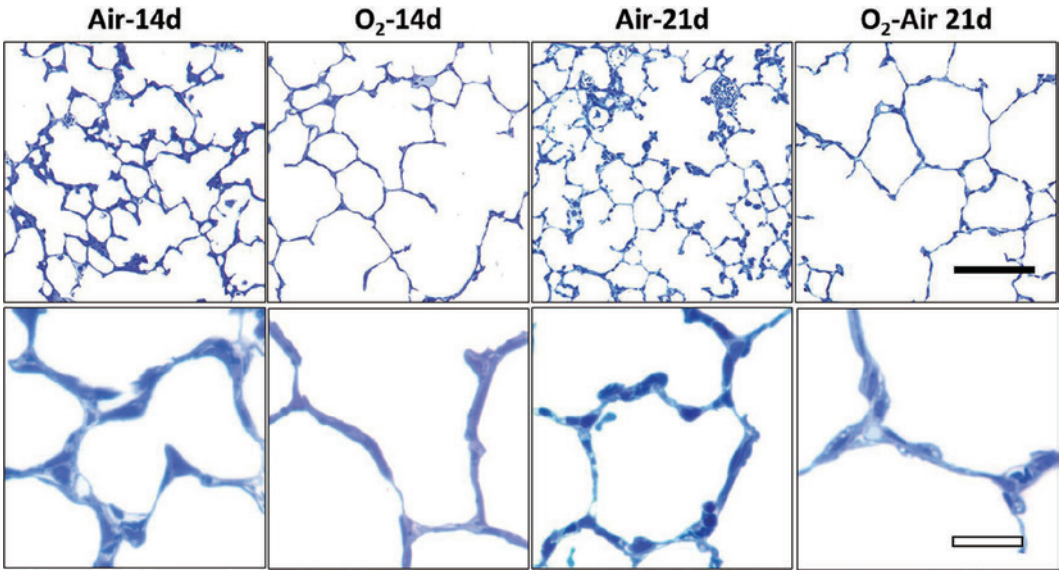

Fig. 1 Effects of hyperoxia on alveolar development. Toluidine blue staining of lung sections from animals exposed to 85% oxygen for 14 days (O_2-14d) indicated larger distal airspace areas and fewer secondary septa as compared to air-exposed control lungs (Air-14d and Air-21d). These abnormal structural changes persisted even under normal air replacement conditions (for 7 days) after hyperoxia (O_2-Air 21d). Closed scale bar, 100 μm; open scale bar, 20 μm

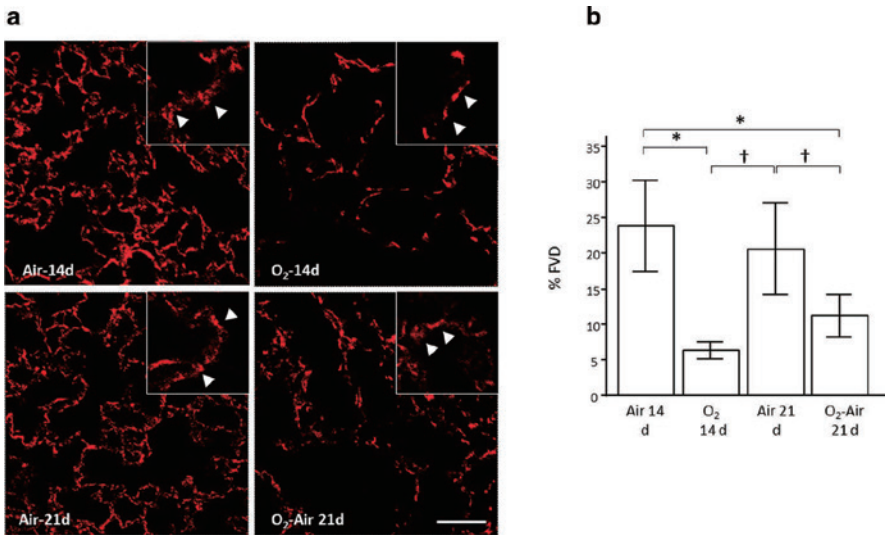

Fig. 2 Quantification of the effects of hyperoxia on pulmonary micro- vasculature in newborn mouse lungs. **a** CD31 immunofluorescence staining of pulmonary microvascular endothelial cells in the periph- ery of 14- and 21-day-old mouse pup lungs treated as indicated. Compared to air-exposed lungs (Air-14d), lungs exposed to 85% oxy- gen (O_2-14d) presented a lower CD31 signal. CD31 staining was par- tially restored in animals subjected to normal air replacement condi- tions after hyperoxic exposure (O_2-Air 21d), but did not reach control levels (Air-21d). Arrow heads in insets indicate blood vessels. Scale bar, 75 μm. **b** Chronic exposure to 85% oxygen (O_2-14d) caused a decrease in the percentage of fluorescent volume density (% FVD) of endothelial cells in the peripheral lung. In the lungs of animals subjected to normal air replacement conditions after hyperoxia (O_2-Air 21d), % FVD partially improved, but did not reach control levels (Air-21d). Data are expressed as means ± SDs; $^*P < 0.05$ vs. Air-14d, $^\dagger P < 0.05$ vs. Air-21d; $n = 6$ in each group

when compared with that of normally developing lungs (Air-21d).

As shown in Fig. 3, ultrastructural analysis of pulmonary capillaries at the cellular level revealed that chronic exposure to 85% oxygen disrupted normal microvascular structure, especially with regard to EC layer components. ECs presented a heterogeneously thick and irregular cytoplasm, with well-developed basal infoldings. Moreover, red blood cells (RBCs) inside the alveolar capillary seemed to be stuck in the capillary lumen, suggesting collapsed capillaries and altered pulmonary microcirculation. BABs from injured lungs, comprising EC, AEC, and the basal lamina, were much thicker than those of air-exposed lungs, and most BABs were filled with abnormal mitochondria-rich EC layers. In contrast, BAB basal lamina layers in hyperoxia-exposed lungs were not significantly different from those in controls. Even in the lungs of animals exposed to normal air replacement conditions, ECs presented a heterogeneously thick cytoplasm rich in organelles, collapsed alveolar capillaries, and EC layers occupying most of the BABs.

To confirm these ultrastructural findings, BABs, ECs, and AECs were quantified. As shown in Fig. 4a, b, exposure to 85% oxygen (O_2-14d) was associated with a 2.5-fold increase in BAB thickness as compared with air-control animals (Air-14d). The proportion of EC components in the BAB was 1.8-fold higher in hyperoxia-exposed (O_2-14d) than in air-breathing (Air-14d) lungs. In animals exposed to a 7-day recovery under normal air replacement conditions (O_2-Air 21d), BAB thickness and the proportion of EC components in BABs were lower than in hyperoxia-exposed animals, but they did not return to air-control levels (Air-21d). Additionally, as shown in Fig. 4c, EC mean cytoplasm thickness was 3.5-fold higher, and the standard deviation (SD) of EC cytoplasm per capillary was 6.5-fold larger in hyperoxia-exposed than in air-breathing lungs. These results suggested that ECs in the injured developing lung present a heterogeneously thick and irregular cytoplasm, resulting in the collapse of alveolar capillaries. Following exposure to normal air replacement conditions after hyperoxic exposure, EC cytoplasm thickness partially improved as compared to oxygen-exposed lungs, but the SD per capillary remained larger than that of air-control lungs (Fig. 4d). As shown in Fig. 3, the thickness of the basal lamina layer in BAB was similar between the groups (Air-14d, 0.05 ± 0.01; O_2-14d, 0.07 ± 0.02; Air-21d, 0.05 ± 0.003; and O_2-Air, 21d 0.05 ± 0.030 μm; $P = 0.34$).

Hyperoxic exposure increases pulmonary artery thickness and RV mass index

To estimate the progression of secondary PH caused by hyperoxia, we examined the structure of pulmonary

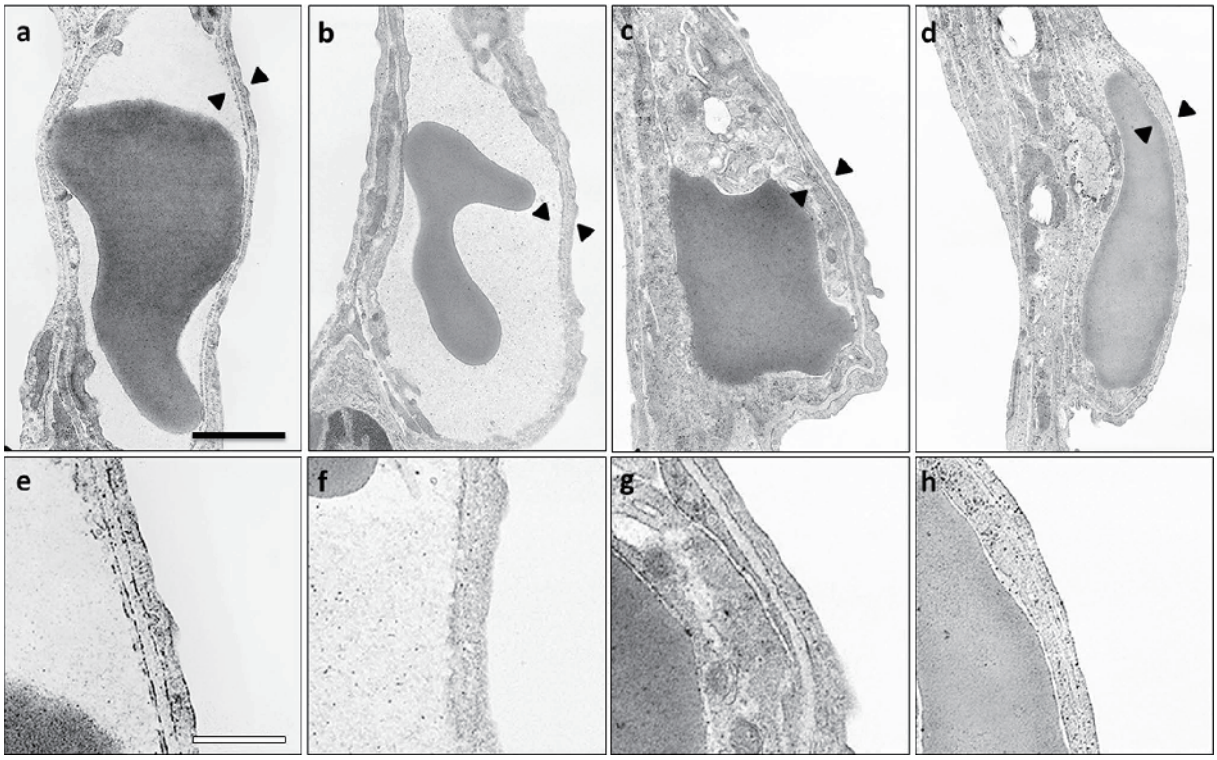

Fig. 3 Transmission electron microscopic ultrastructure of pulmonary endothelial cells (ECs). **a, b** Pulmonary capillaries in air-breathing pup lungs (Air-14d, Air-21d) displayed thin blood–air barriers (BABs) and a wide capillary lumen with red blood cells inside. ECs in the alveolar capillary had thin and uniform cytoplasm. **c** Pulmonary capillaries of hyperoxia-exposed pup lungs (O_2-14d) displayed remarkably thick BABs and a collapsed capillary lumen, made of ECs with a heterogeneously thick cytoplasm. **d** Pulmonary capillaries from animals subjected to normal air replacement conditions after hyperoxia (O_2-Air 21d) presented partially restored thin BABs, but persistent abnormal EC morphology and a heterogeneously thick cytoplasm. Scale bar (black), 1.0 µm. **e, f** Under higher magnification, BABs from air-breathing pup lungs (Air-14d and Air-21d) displayed a clearly differentiated three-layered structure comprised alveolar epithelial cells (AECs), basement membrane (BM), and ECs. **g** In hyperoxia-exposed lungs (O_2-14d), BABs were much thicker, and interestingly, ECs occupied most of the space. **h** Normal air replacement conditions after hyperoxia (O_2-Air 21d) appeared to partially restore BAB thickness. Scale bar (white), 0.35 µm. Black arrowheads denote the parts of BABs magnified in the lower panels

arteries associated with terminal bronchioles and respiratory bronchioles [14, 27, 28], as well as RV hypertrophy. As shown in Fig. 5, the ED of the pulmonary artery was similar between all groups (Air-14d, 43 ± 6; O_2-14d, 41 ± 11; Air-21d, 50 ± 9; and O_2–Air 21d, 51 ± 9 µm; $P = 0.16$). Exposure to 85% oxygen for 14 days caused a 2.5-fold increase in MT% relative to control animals. Compared to hyperoxia-exposed lungs, the lungs of animals subjected to normal air replacement conditions after hyperoxic exposure showed a partial decrease in MT%, but without reaching control levels (Fig. 5b). As shown in Fig. 5c, exposure to 85% oxygen for 14 days caused a 1.4- fold increase in the RV/(LV + S) weight ratio as compared to the air-control ratio. Even in animals subjected to nor- mal air replacement conditions after hyperoxic exposure, the RV/(LV + S) weight ratio remained high and failed to return to the air-control level.

Discussion

This study aimed to investigate the morphological characteristics of pulmonary vascular disease secondary to BPD. This is caused by oxygen toxicity and can be mitigated by subsequent normal air replacement. Actually previous animal studies have shown that exposure to hyperoxia in the neonatal period causes lung structural changes that are similar to the histology seen in human infants with BPD; that is, reduced complexity of the distal lung with decreased alveolar number and vascular growth [2, 4–7]. We found that continuous inhalation of a high level of oxygen by newborn mice during the terminal stage of lung development disrupted the pulmonary microvasculature at the cellular level. In particular, ECs in the alveolar wall presented a heterogeneously thick and irregular cytoplasm,

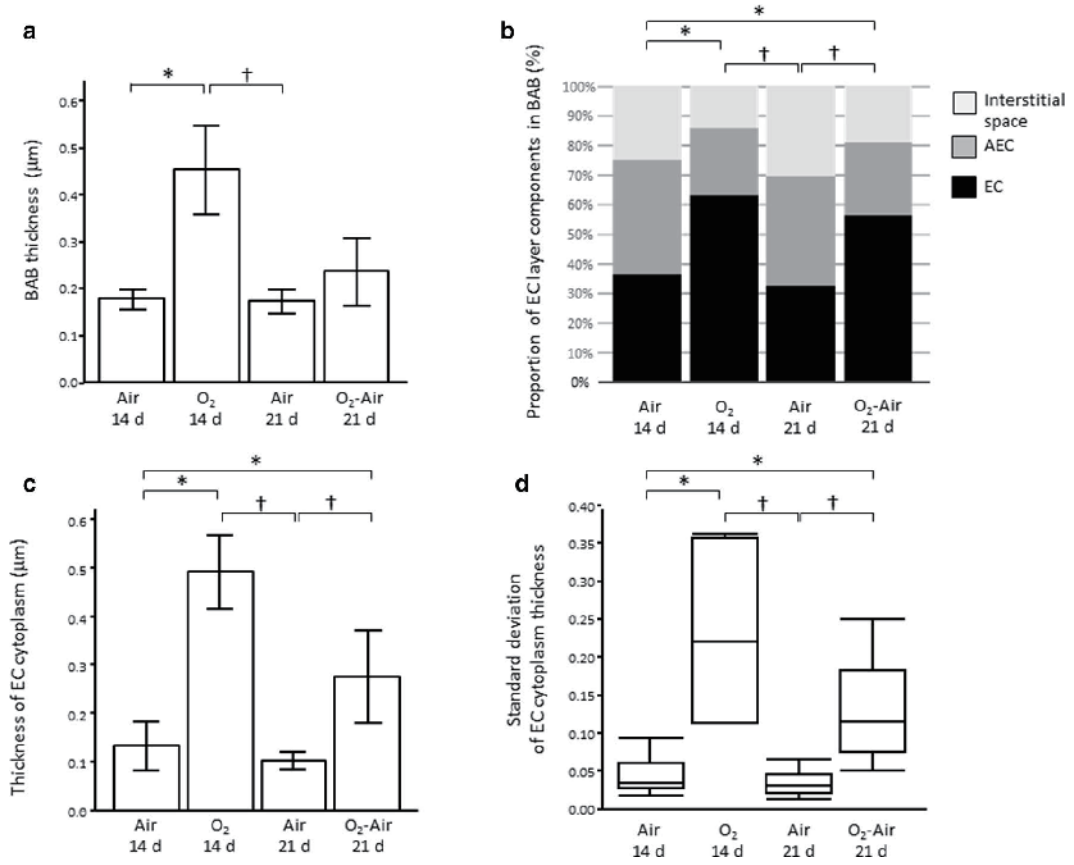

Fig. 4 Quantification of ultrastructural changes during alveolar development. **a** BAB thickness was measured in each group using five different portions of BAB per capillary, and the mean value was calculated. Normal air replacement conditions (O_2-Air 21d) partially restored the low BAB thickness of hyperoxia-exposed lungs (O_2-14d). **b** The proportion of EC layer components in BABs was calculated in each group. In air-exposed pup lungs, BAB was composed of three clearly visible layers consisting of AECs, BM, and ECs. In hyperoxia-exposed lungs (O_2-14d), BAB was mostly occupied by ECs. In the group subjected to normal air replacement conditions after hyperoxia (O_2-Air 21d), BAB was still occupied by a thick EC layer. **c** The mean thickness of EC cytoplasm per pulmonary capillary was measured and calculated for each group. We measured five different cytoplasmic portions of EC per lung and calculated the mean value. Normal air replacement conditions (O_2-Air 21d) partially restored the increased EC cytoplasm thickness of hyperoxia-exposed lungs (O_2-14d). **d** SD of the thickness of EC cytoplasm, measured at five different points per capillary. Hyperoxic exposure (O_2-14d) was associated with large SD values compared with air-exposed lungs (Air-14d); SD remained high even after exposure to normal air replacement conditions (O_2-Air 21d). Data are expressed as means± SDs (a, b, c) or medians (d); $^*P < 0.05$ vs. Air-14d, $^\dagger P < 0.05$ vs. Air-21d; $n = 6$ capillaries per group

causing the capillary lumen to collapse. In addition, BABs were significantly thicker than those of air-control lungs, possibly because of a remarkable increase in EC layer components. Furthermore, even in the peripheral lungs of animals subjected to normal air replacement conditions after hyperoxic exposure, ECs maintained the abnormal morphology. In adult rodent models of hyperoxic lung injury, a persistent abnormal morphology of ECs and BABs accompanied by increased subcellular organelles was still observed in normal air replacement conditions after hyperoxia [15, 17]. These impairments of pulmonary vasculature may cause serious pulmonary vascular diseases such as secondary PH.

BPD complicated with PH is one of the significant independent risk factors for delayed neurodevelopmental outcome in premature infants, and should be prevented for intact survival of premature infants [11]. Actually, our animal models of pulmonary microvascular injuries accompanied by persistent increased pulmonary arterial medial thickness and right ventricular hypertrophy even after exposure to normal air replacement conditions might depict PH with BPD. Therefore, these animal experiments could be the ideal model to find out the treatment strategy for PH with BPD in future study.

Our study is unique in that we focused on the ultrastructural characterization of the pulmonary microvasculature

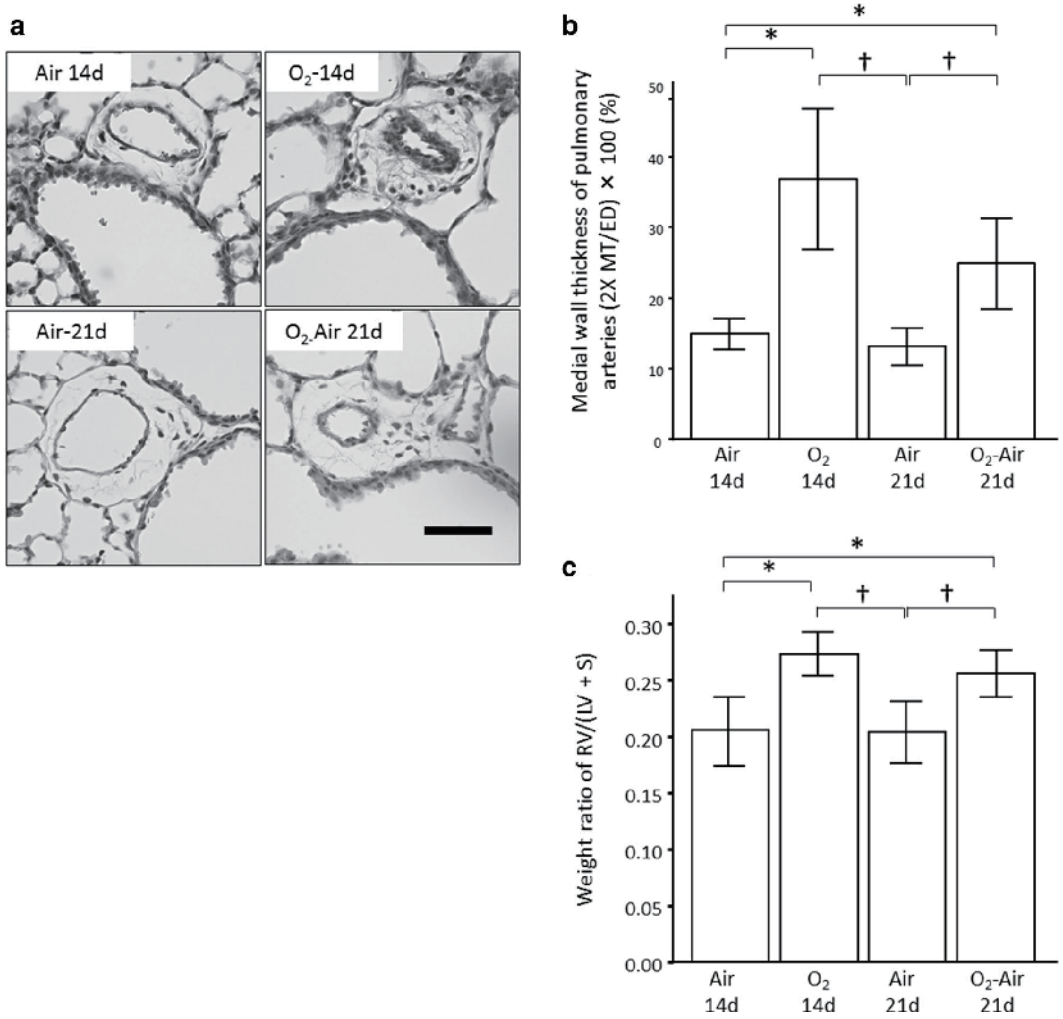

Fig. 5 Effect of hyperoxia on the thickness of pulmonary arteries associated with terminal and respiratory bronchioles. **a** H&E-stained lung sections indicating the thickness of pulmonary arteries associated with terminal and respiratory bronchioles. Hyperoxic exposure (O_2-14d) was associated with increased medial wall thickness of pulmonary arteries. Normal air replacement conditions after hyperoxia (O_2-Air 21d) failed to decrease medial wall thickness when compared with air-breathing lungs (Air-21d). Scale bar, 50 μm. **b** Medial wall thickness was measured on pulmonary arteries associated with terminal bronchioles and respiratory bronchioles (20–100 μm) using the same sections depicted in (**a**). Three vessels per pup lung were assessed for medial thickness (MT) and external arterial diameter (ED). MT was expressed as a percentage of ED, MT% = [MT × 2 × 100]/ED. Hyperoxic exposure (O_2-14d) was associated with increased MT% at approximately 40–50-μm diameter of the pulmonary artery as compared to air exposure (Air-14d and Air-21d). MT% in lungs subjected to normal air replacement conditions (O_2-Air 21d) was still higher than that in air-breathing lungs (Air-21d). Data are expressed as means ± SDs; $^*P < 0.05$ vs. Air-14d, $^\dagger P < 0.05$ vs. Air-21d; $n = 6$ for each group. **c** Assessment of right ventricular hypertrophy. Hearts were removed and dissected to separate the free wall of the right ventricle (RV) from the left ventricle (LV) and septum (S). RV hypertrophy was calculated as the RV/(LV + S) weight ratio. Hyperoxic exposure (O_2-14d) was associated with increased RV/(LV + S), compared with the air-control (Air-14d). Exposure to normal air replacement conditions after hyperoxia (O_2-Air 21d) did not significantly lower the RV/(LV+ S) value. Data are expressed as means± SDs; $^*P < 0.05$ vs. Air-14d, $^\dagger P < 0.05$ vs. Air-21d; $n = 4$ for each group

specifically in the injured developing mouse lung. In addition, our results on the ultrastructural changes in ECs and BABs were confirmed by morphometric analyses, suggesting that ECs in the alveolar wall might represent not only the main site of injury but also a therapeutic target in the injured developing lung. Ultrastructural changes in pulmonary microvasculature in lungs injured by hyperoxia exposure or antiangiogenic drug administration have been previously reported; however, TEM revealed the contradictory results [15–18]. Kistler et al. [16] demonstrated that BAB

thickness in adult rat lungs was remarkably increased after 48 h of exposure to hyperoxia. This was attributed largely to the progressive enlargement of the interstitial space rather than thicker EC layers, as demonstrated in our newborn mice models. Cho et al. [18] have reported enlarged capillaries with multiple RBCs in the lumen in developing mouse lungs injured by antiangiogenic agents, while studies on injured developing rat lungs have reported the disruption of endothelial tight junctions [29, 30], a phenomenon we could not confirm at the cellular level in 14-day hyperoxia-exposed newborn mouse lungs. This apparent discrepancy might be because of differences in animal age (newborn or adult), oxygen exposure time and concentration, and the timing of injury. In particular, we exposed developing mouse lungs to hyperoxia for 14 days after birth, in both the saccular and alveolar stages, and our injury model might be more severe than others.

The ultrastructural changes observed in the present study might contribute to secondary PH in BPD. A possible mechanism involving thick BABs and collapsed alveolar capillaries posits that the former might cause impaired gas exchange and worsen hypoxic or hypercapnia conditions. Ahlfeld et al. [31] demonstrated that impairment of alveolar capillary septal development caused by hyperoxia correlated significantly with reduced functional gas exchange, as determined by carbon monoxide diffusing capacity in neonatal mouse pups. Consequently, their report might support our hypothesis that ultrastructural changes observed in thick BABs correlate with an impaired gas exchange function. The latter causes abnormal vasoreactivity in the pulmonary microvasculature, finally leading to secondary PH, indicated here by the increased RV/(LV + S) weight ratio and thickness of small pulmonary arteries. On the contrary, collapsed alveolar capillaries have been also suggested to impair pulmonary microcirculation by obstructing RBC movement, thus leading to secondary PH. However, pulmonary capillaries in the alveolar wall lack muscular components and offer little resistance. Moreover, as capillary diameter is usually smaller than that of RBCs and the RBCs passing through capillaries are distorted, we should prove the obstructing RBC movement by other methods. Therefore, further research will be needed to confirm this hypothesis.

There are some limitations to our study. Because we exposed developing mouse lungs to hyperoxia in both the saccular and alveolar stages, our BPD model might have exhibited more severe structural changes than other animal models of BPD. Numerous reports have demonstrated that signaling pathways such as the vascular endothelial growth factor and transforming growth factor beta pathways play important roles in vasculogenesis and alveologenesis in the developing lung [4, 12, 13, 32]. The exact mechanisms responsible for microvascular injury to BABs and ECs observed in this study remain unknown. Therefore, further research on abnormal microvasculature should focus on which signal transduction pathways correlate with abnormal EC morphological changes and on how disrupted BABs can be reorganized by modulating these signaling pathways. Our future direction of possible mechanistic targets might be TGF-β signaling pathway. Nakanishi et al. observed that TGF-β signaling was increased in the hyperoxia-exposed mouse pup lung, and that modulation of TGF-β signaling with a neutralizing antibody improved alveolar and microvascular development in newborn mice with hyperoxic lung injury [13]. Furthermore, Bachiller et al. reported that TGF-β might also modulate pulmonary nitric oxide signaling in the injured developing lung [33]. Although our animal model is focusing on lung injuries in more chronic phase than their reports, the strategy for modulation of TGF-β signaling even in later phase of lung injuries might be promising treatment for abnormal structural changes of ECs and BABs.

Conclusion

Pulmonary capillaries in the injured newborn mouse lung presented thick BABs consisting of ECs with abnormal morphology, which persisted following subsequent exposure to normal air replacement conditions. These ultrastructural changes might cause abnormal pulmonary microcirculation and finally lead to secondary PH in BPD. Future studies should focus on novel strategies to modulate signaling pathways involved in EC stability.

Acknowledgements This study was supported by the Medical Research Institute, Tokyo Women's Medical University. We would like to thank
T. Matsuda, Tohoku University, K. Chou, Hokkaido University, and S. Shimizu, Tokyo Women's Medical University, for their excellent support during lung structural analysis in this study. We would like to thank Editage (http://www.editage.jp) for English language editing.

Funding This study was supported by a Takako Satake Research Fel- lowship Grant (Grant Number 54) and the Ministry of Education, Culture, Sports, Science and Technology (MEXT) KAKENHI (Grant Number 16K10111).

Compliance with ethical standards

Conflict of interest Teijin Pharma Ltd., Tokyo, Japan kindly provided the home oxygen condenser (TO-90-7H) without any compensation. They had no control over the interpretation, writing, or publication of this study. The authors have no financial relationships relevant to this article to disclose.

References

1. Husain AN, Siddiqui NH, Stocker JT (1998) Pathology of arrested acinar development in postsurfactant bronchopulmonary dysplasia. Hum Pathol 29:710–717
2. Jobe AH, Bancalari E (2001) Bronchopulmonary dysplasia. Am J Respir Crit Care Med 163:1723–17239

3. Abman SH (2001) Bronchopulmonary dysplasia: “a vascular hypothesis”. Am J Respir Crit Care Med 164:1755–1756
4. Kunig AM, Balasubramaniam V, Markham NE et al (2005) Recombinant human VEGF treatment enhances alveolarization after hyperoxic lung injury in neonatal rats. Am J Physiol Lung Cell Mol Physiol 289:L529–L535
5. Lin YJ, Markham NE, Balasubramaniam V et al (2005) Inhaled nitric oxide enhances distal lung growth after exposure to hyperoxia in neonatal rats. Pediatr Res 58:22–29
6. Wilson WL, Mullen M, Olley PM et al (1985) Hyperoxia-induced pulmonary vascular and lung abnormalities in young rats and potential for recovery. Pediatr Res 19:1059–1067
7. de Visser YP, Walther FJ, Laghmani el H et al (2009) Sildenafil attenuates pulmonary inflammation and fibrin deposition, mortality and right ventricular hypertrophy in neonatal hyperoxic lung injury. Respir Res 10:30
8. Bhat R, Salas AA, Foster C et al (2012) Prospective analysis of pulmonary hypertension in extremely low birth weight infants. Pediatrics 129:e682–e689
9. Khemani E, McElhinney DB, Rhein L et al (2007) Pulmonary artery hypertension in formerly premature infants with bronchopulmonary dysplasia: clinical features and outcomes in the surfactant era. Pediatrics 120:1260–1269
10. Slaughter JL, Pakrashi T, Jones DE et al (2011) Echocardiographic detection of pulmonary hypertension in extremely low birth weight infants with bronchopulmonary dysplasia requiring prolonged positive pressure ventilation. J Perinatol 31:635–640
11. Nakanishi H, Uchiyama A, Kusuda S (2016) Impact of pulmonary hypertension on neurodevelopmental outcome in preterm infants with bronchopulmonary dysplasia: a cohort study. J Perinatol 36:890–896
12. Bhatt AJ, Pryhuber GS, Huyck H et al. (2001) Disrupted pulmonary vasculature and decreased vascular endothelial growth factor, Flt-1, and TIE-2 in human infants dying with bronchopulmonary dysplasia. Am J Respir Crit Care Med 15;164:1971–1980
13. Nakanishi H, Sugiura T, Streisand JB et al (2007) TGF-β neutralizing antibodies improve pulmonary alveologenesis and vasculogenesis in the injured newborn lung. Am J Physiol Lung Cell Mol Physiol 293:L151–L161
14. Roberts RJ, Weesner KM, Bucher JR (1983) Oxygen-induced alterations in lung vascular development in the newborn rat. Pediatr Res 17:368–375
15. Mastin JP, Shelburne JD, Thet LA (1988) Subcellular changes in capillary endothelial cells during repair of hyperoxic lung injury. J Appl Physiol 64:689–696
16. Kistler GS, Caldwell PR, Weibel ER (1967) Development of fine structural damage to alveolar and capillary lining cells in oxygen-poisoned rat lungs. J Cell Biol 32:605–628
17. Durr RA, Dubaybo BA, Thet LA (1987) Repair of chronic hyperoxic lung injury: changes in lung ultrastructure and matrix. Exp Mol Pathol 47:219–240
18. Cho SJ, George CL, Snyder JM et al (2005) Retinoic acid and erythropoietin maintain alveolar development in mice treated with an angiogenesis inhibitor. Am J Respir Cell Mol Biol 33:622–628
19. Berger J, Bhandari V (2014) Animal models of bronchopulmonary dysplasia. The term mouse models. Am J Physiol Lung Cell Mol Physiol 307:L936–L947
20. Tschanz SA, Burri PH (2002) A new approach to detect structural differences in lung parenchyma using digital image analysis. Exp Lung Res 28:457–471
21. Rasband WS. ImageJ, Bethesda, (2015) Maryland USA1997-2012 [cited 2015 August 12]. Available from: http://imagej.nih.gov/ij/
22. Weibel ER (1979) Stereological methods. Academic Press, London
23. Hislop A, Reid L (1976) New findings in pulmonary arteries of rats with hypoxia-induced pulmonary hypertension. Br J Exp Pathol 57:542–554
24. Pappas CT, Obara H, Bensch KG et al (1983) Effect of prolonged exposure to 80% oxygen on the lung of the newborn mouse. Lab Invest 48:735–748
25. Warner BB, Stuart LA, Papes RA et al (1998) Functional and pathological effects of prolonged hyperoxia in neonatal mice. Am J Physiol 275:L110–L117
26. Bucher JR, Roberts RJ (1981) The development of the newborn rat lung in hyperoxia: a dose-response study of lung growth, maturation, and changes in antioxidant enzyme activities. Pediatr Res 15:999–1008
27. Randell SH, Mercer RR, Young SL (1990) Neonatal hyperoxia alters the pulmonary alveolar and capillary structure of 40-day-old rats. Am J Pathol 136:1259–1266
28. Shaffer SG, O’Neill D, Bradt SK et al (1987) Chronic vascular pulmonary dysplasia associated with neonatal hyperoxia exposure in the rat. Pediatr Res 21:14–20
29. Li C, Fu J, Liu H et al (2014) Hyperoxia arrests pulmonary development in newborn rats via disruption of endothelial tight junctions and downregulation of Cx40. Mol Med Rep 10:61–67
30. Hou A, Fu J, Yang H et al (2015) Hyperoxia stimulates the transdifferentiation of type II alveolar epithelial cells in newborn rats. Am J Physiol Lung Cell Mol Physiol 308:L861–L872
31. Ahlfeld SK, Gao Y, Conway SJ et al (2015) Relationship of structural to functional impairment during alveolar-capillary membrane development. Am J Pathol 185:913–919
32. Maniscalco WM, Watkins RH, Pryhuber GS et al (2002) Angiogenic factors and alveolar vasculature: development and alterations by injury in very premature baboons. Am J Physiol Lung Cell Mol Physiol 282:L811–L823
33. Bachiller PR, Nakanishi H, Roberts JD Jr (2010) Transforming growth factor-beta modulates the expression of nitric oxide signaling enzymes in the injured developing lung and in vascular smooth muscle cells. Am J Physiol Lung Cell Mol Physiol 298:L324-L334. https://doi.org/10.1152/ajplung.00181.2009

新生仔マウス高濃度酸素暴露肺障害モデルにおける肺胞微小血管障害の形態学的特徴

北里大学医学部附属新世紀医療開発センター先端医療領域開発部門新生児集中治療学
中西（ナカニシ）　秀彦（ヒデヒコ）

早産児では，さまざまな要因で肺胞および肺胞微小循環系の発達が障害を受け慢性肺疾患（chronic lung disease：CLD）へと進行し，新生児期のみならず長期にわたる呼吸・循環障害を合併する．CLD におけるこの微小血管障害のメカニズムを解明するために，形態学的手法を用いて超微形態評価を行った．新生仔 ICR マウスを出生直後より 14 日間，85％高濃度酸素もしくはルームエア下に暴露させた後に，回復期としてルームエア下に 7 日間留置した．生後 14 日，生後 21 日の固定肺サンプルを用いて，肺胞微小循環系の超微形態解析と，分子生物学的解析，および肺高血圧の評価を行った．

高濃度酸素暴露群における肺胞毛細血管は，内腔が虚脱しており，不均一に肥厚した細胞質成分を伴う異常構造を有した血管内皮細胞を認めた．正常ルームエアコントロール群と比較して，血液空気関門は著明に肥厚しており，その成分の多くを肥厚した血管内皮細胞が占めていた．またこの微小形態異常に伴い，高濃度酸素暴露群では肺動脈中膜成分の肥厚と右室心筋重量の増大を認めた．この超微形態異常，肺動脈中膜肥厚，右室心筋重量の増大は 7 日間の回復期においても遷延していた．これら結果より，肺胞微小血管系における血管内皮細胞の形態異常と血液空気関門の肥厚が，肺動脈リモデリングと右室肥大と関連があることが示唆された．これら超微形態変化が，CLD に続発する二次性肺高血圧の発症機序の一因である可能性があり，さらなる治療法の検索を模索している．

本論文は日本臨床分子形態学会の許諾を得て Medical Molecular Morphology より転載しております．